Modeling, simulation and experimental validation of a pad humidifier used in solar desalination process

K. Zhani[a,*], H. Ben Bacha[b]

[a]LASEM (LAboratoire des Systèmes Electro-Mécaniques), National Engineering School of Sfax, B.P. W3038 Sfax, Tunisia
Email: zhani_khalifa@yahoo.fr
[b]College of Engineering at Alkharj, Salman Bin Abdulaziz University, Alkharj B.P. 655-11946, Kingdom of Saudi Arabia

ABSTRACT

Water is an extremely important commodity for the improvement of arid and semi-arid environments. As for the water production technology, desalination techniques based on either thermal or membrane separation methods such as multi-stage flash, multi-effect, vapor compression and reverse osmosis are only reliable for large capacity ranges of 100–50,000 m^3/day of freshwater production, inefficient from the view point of energy consumption and generally coupled to fossil fuel sources that have a negative impact on the environment. Hence, for the improvement of these regions it is necessary to shift from fossil fuel usage to some environmentally friendly energy source, such as solar energy, as it is available abundantly in such environments. The aim of the present paper is to study numerically and experimentally a pad humidifier used in a seawater solar desalination unit based on humidification–dehumidification principle. The pad humidifier dynamic modeling is based on various heat and mass balance equations. The effect of operating parameters on the pad humidifier characteristics has been investigated. To validate the computer program, a comparison between the experimental and theoretical results was conducted, and a good agreement had been obtained.

Keywords: Solar desalination; Pad humidifier; Dynamic modeling; Simulation and experimental validation

1. Introduction

Nowadays, most of the countries in the Middle East and North Africa regions are suffering from the acute problem of fresh water scarcity due to limited water resources and aridity. There are many ways to solve the water shortage problem depending on the location, such as transportation of water between different areas, reusing of wastewater in industry and agriculture, and improving management of water resource. Tunisia, like many other countries throughout the world, has given high priority to desalination of seawater and brackish water as a source of water for domestic, industrial and agricultural applications.

*Corresponding author.

Conventional desalination techniques such as multi-stage flash, multi-effect, vapor compression and reverse osmosis are only reliable for large capacity ranges of 100–50,000 m^3/day of freshwater production [1]. These technologies are costly for small amounts of fresh water, inefficient from the viewpoint of energy consumption and require high maintenance due to the practical difficulties associated with the high operating temperature, such as corrosion and scale formation. Moreover, the use of conventional energy sources to drive these technologies has a negative impact on the environment due to gas emissions, especially CO_2. Coupling renewable energy sources, such as solar energy, with desalination units would generate a sustainable source of freshwater as well as energy. This coupling is highly valued as it limits and reduces the consumption of fossil fuel and the production of CO_2 emissions.

Compared with conventional desalination techniques, solar desalination units based on humidification–dehumidification principle are characterized by their limited production of freshwater. Therefore, to optimize the functioning and then the productivity of solar desalination units, we should first study in depth the behavior of each component constituting the unit. For this purpose, according to literature review, many investigators developed and studied different components of various solar desalination systems using the humidification–dehumidification principle.

In 2011, Kassim et al. [2] have focused numerically the effect of inlet air humidity on an upward airflow in a humidifier intended for a humidification and dehumidification desalination system. A vertical parallel-plate channel constitutes the humidifier. One of the plates is wetted by a liquid water film and maintained at a constant temperature, while the other is dry and thermally insulated. The airflow enters the channel with constant temperature, humidity and velocity. It was found that the increase in air humidity at the channel entrance affects seriously the performances of the humidifier as it induces condensation of the water vapor on the walls. On the other hand, it was stated that the humidifier works well for low inlet humidity.

In 2010, Marmouch et al. [3] have investigated experimentally the thermal performance of a forced cooling tower used in a solar desalination system based on humidification–dehumidification of air. The cooling tower is a counter flow wet one filled with film packing materials. Experimental results show that the tower characteristic decreases with an increase in the water/air mass flow ratio. They have also developed correlations expressing the variation of the tower characteristic with the liquid to gas mass flow rate ratio for three inlet water temperatures.

In 2004, Bourouni et al. [4] has studied theoretically heat and mass transfers in a horizontal-tube falling-film condenser used in an innovative desalination plant. The polypropylene exchanger was designed to work at relatively high temperatures (25–35℃). The elaborated model is based on the resolution of heat and mass transfer equations in each cell of the exchanger. The predicted transfer characteristics obtained from the simulations were compared with experimental data. The influence of the different thermal, hydrodynamic and geometric parameters on the condenser performances was investigated. An increase in condensing exchanger performance was found when the inlet cooling water decreases and air velocity increases. For the conditions corresponding to the real environment of southern Tunisia, the model predicted that the amount of condensed water cannot exceed 2 m^3/day.

In the same year, Ben Amara et al. [5] conducted an experimental and theoretical study of a pad humidifier used in a new multi-stage solar desalination process in operation in Tunisia. The experimental operation of the humidifier is presented in terms of temperature, relative and absolute humidity, and the quantity of evaporated water for different climatic and working conditions. The air was slightly saturated at the exit of the humidifier, independent of the climatic conditions; the air temperature was slightly greater than the water temperature at the outlet of the humidifier during a sunny day. The numerical study was in good agreement with the experimental results.

In 2003, two types of air humidifiers, namely a tubular spray humidifier, and a pad humidifier were experimentally compared and simulated as a part for a multi-stage solar desalination process by Yanniotis et al. [6]. They demonstrated that the pad humidifier is the most efficient and is more suitable for use to enrich air with water vapor in the new desalination process.

The pad humidifier, object of this article, is one of the five components (air solar collector, water solar collector, humidifier, evaporation tower and condensation tower) of solar desalination unit that is shown in Fig. 1. The performance of the humidifier depends mainly on the design and operating parameters. However, to estimate the optimum values of these parameters in different operating conditions using full experiments is costly and time-consuming. Therefore, the development of a simulation model offers a better alternative and has proven to be a powerful tool in the evaluation of the performance of the system.

In three previous papers [7–9], we present the detailed study of each unit components and the effect of different operating modes on freshwater production in steady state regime. The paper at hand deals with mathematical modeling in dynamic regime and exper-
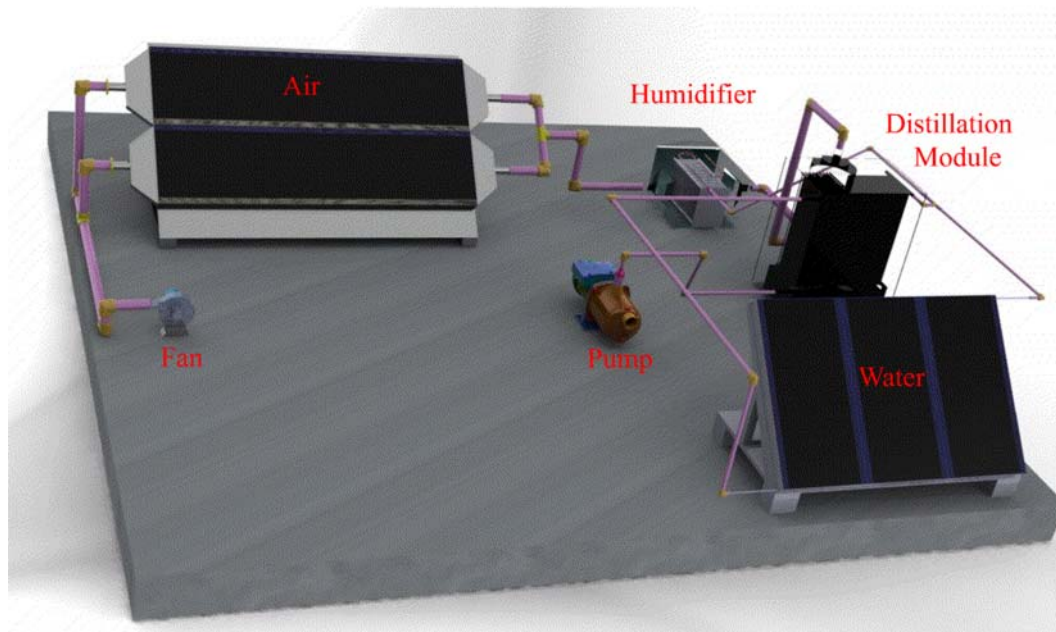
Fig. 1. A 3-D view of the solar desalination unit.

imental validation of a humidifier used in water desalination unit based on the humidification–dehumidification principle. Its underlying objectives are:

- To develop a dynamic mathematical model capable of predicting the thermal performance of the humidifier.
- To present numerical and experimental data as an example of the validation process that has been carried out to assess the credibility of the numerical models.

2. Humidifier design and instrumentation

Humidifiers, also called cooling towers, are used in many chemical processes. In the desalination process, the humidifier is used to separate clean water from the salt water. This is essentially an extraction process. The humidifier used in the desalination prototype is a pad one. The cross-sectional area of the pad is 0.6×0.8 m, while its height is 0.56 m. At the top, there is a liquid distributor, which can feed the pad with hot brackish water coming from water solar collectors, while at the bottom there is a liquid collector, where brine is collected as it drains down the pad. Thus, the hot brackish water flows downward, while the air passes in a cross-flow direction. Textile

(Viscose) of a $14 \, m^2$ ($52 \, m^2/m^3$) surface is used as packing to increase the interface area between the air and water, which form the wetted surface. On the outside, the humidifier is covered with a polyethylene sheet of thickness 15 mm and insulated with a layer of armaflex (see Fig. 2).

The measured variables in the experiments reported in this paper include inlet and outlet fluid (air and water) temperatures and the climatic conditions (ambient temperature and the solar irradiation). The humidifier was instrumented with Pt 100 thermistors with a sensibility of $0.3799 \, \Omega/°C$ for measuring the outlet and the inlet water temperatures and ambient temperature. The Pt 100, which measured the ambient temperature, was kept in a shelter to protect the sensor from direct sunlight. The outlet and the inlet of both relative humidity and air temperatures in the humidifier were measured using the TH100 transmitter with sensibilities of $0.160 \, mA/°C$ and $0.159 \, mA/\%$ respectively of temperature and relative humidity. A pyranometer, with 1% accuracy and $12.29 \, \mu V/Wm^2$ sensibility, was used to measure the total solar irradiation placed in a horizontal plane adjacent to the collector. All the sensors, which were calibrated before using to determine the probes sensibility, were connected to a data acquisition system (type Agilent 34970A). During experimentation, all the parameters were measured and recorded every 1 min for up to 420 mn. All the measurements started at 10:30 a.m.
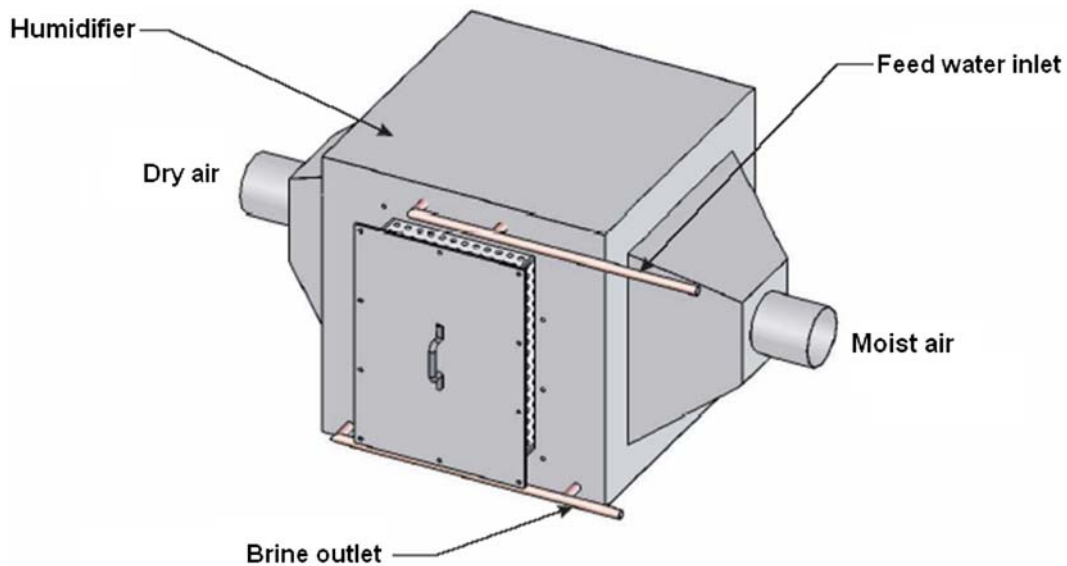
Fig. 2. Schematic diagram of the humidifier designed with Solidworks.

3. Humidifier mathematical modeling

Mathematical modeling is at the very core of the design and optimization process for thermal systems because the mathematical model brings out the important variables and the governing parameters. The humidifier can be dynamically modeled as shown in Fig. 3. The humidifier is nourished at the top by the hot salt water coming from the solar sensor with a temperature $T_{L2}(t)$ and leaves at the bottom of the section at a temperature $T_{L1}(t)$. Air is introduced at the right side of the humidifier at a temperature $T_{g1}(t)$ and a specific humidity $W_{g1}(t)$. Air leaves at the left side of the humidifier at a temperature $T_{g2}(t)$, a specific humidity $W_{g2}(t)$. The mass velocity of air is $m_g(t)$. The mass velocities of the water at the outlet and inlet are, respectively, $m_{L1}(t)$ and $m_{L2}(t)$.

The method of setting up the mass, thermal and enthalpy balances will be undertaken with the following simplifying assumptions:

- The process is adiabatic,
- The air and water flows are in countercurrent and one-dimensional,
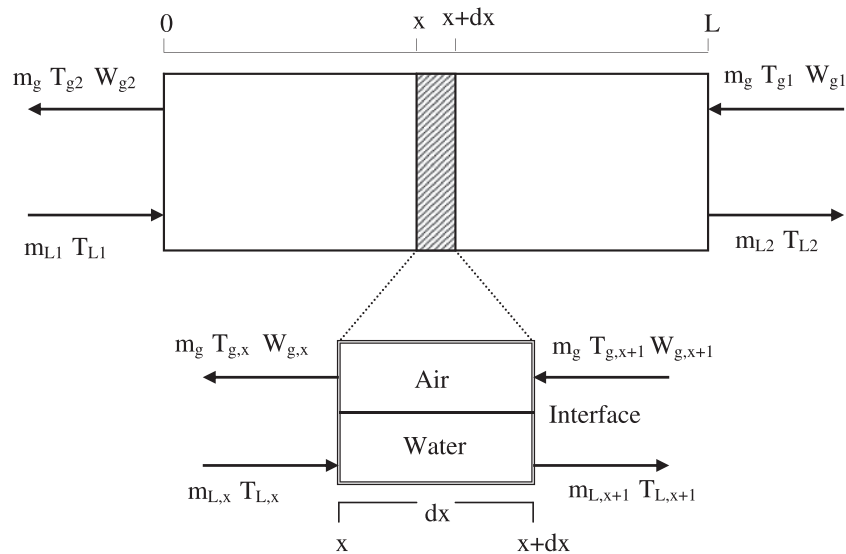

Fig. 3. An element of volume of the humidifier.

- The specific heat of water is constant during its passage by the humidifier,
- The equations are written as if the transfer were from water to air.

Consider a differential width, *dx*, across the contacting area as shown in Fig. 3, which shows the differential section of the contacting area is divided into three control volumes—air, water and interface—to set up the heat and mass balance equations.

Water phase

The thermal balance of water in the humidifier length volume element *dx* and during the interval of time *dt* is given by the following equation:

[The quantity of energy accumulated in the length volume element *dx*] = [(the quantity of energy carried by water during *dt* time) − (the quantity of energy transmitted toward the surface of separation water–air during *dt*)]

Mathematically, this can be expressed as:

$$M_l C_l dT_l dx = m_l C_l dT_l dt - h_l a_h (T_i - T_l) dx dt \qquad (1)$$

It can be further simplified as:

$$\frac{\partial T_l}{\partial t} = \frac{m_l}{M_l} \frac{\partial T_l}{\partial x} - \frac{h_l a_h}{M_l C_l} (T_i - T_l) \qquad (2)$$

Air phase

The air thermal balance in the humidifier length volume element *dx* and during the interval of the time *dt* is the following one:

[The quantity of energy accumulated in the volume length element *dx*] = [(the quantity of energy received by the surface of separation water–air during the interval of time *dt*) − (the quantity of energy transferred toward the air flow rate during *dt*)]

Mathematically, this can be expressed as:

$$M_g C_g dT_g dx = h_g a_h (T_i - T_g) dx dt - m_g C_g dT_g dt \qquad (3)$$

It can be further simplified as:

$$\frac{\partial T_g}{\partial t} = -\frac{m_g}{M_g} \frac{\partial T_g}{\partial x} - \frac{h_g a_h}{M_g C_g} (T_g - T_i) \qquad (4)$$

Water–air interface

The heat balance at air–water interface is given by the following equation:

[The quantity of energy transferred from the water current through the liquid film toward the water–air interface] = [(the quantity of heat transmitted from the surface of separation through the air film toward the air current) + (the quantity of heat provided to evaporate the water mass quantity transferred of the liquid through the interface toward the air current)]

Mathematically, this can be expressed as:

$$h_l a_h (T_i - T_l) = h_g a_h (T_i - T_g) + \lambda_o K_m a_h (W_i - W_g) \qquad (5)$$

The balance of mass at the level of air–water interface is given by the following equation:

[The quantity of steam accumulated]
 = [(the mass water quantity transferred from the interface through the air film toward air current during *dt*) − (the produced quantity of steam transmitted to air current during *dt*)]

Mathematically, this can be expressed as:

$$M_g dW_g dx = K_m a_h (W_i - W_g) dx dt - m_g dW_g dt \qquad (6)$$

It can be further simplified as:

$$\frac{\partial W_g}{\partial t} = -\frac{m_g}{M_g} \frac{\partial W_g}{\partial x} + \frac{K_m a_h}{M_g} (W_i - W_g) \qquad (7)$$

To be numerically integrated, the above-mentioned equations are completed with both empirical correlations of the voluminal heat coefficients ($h_l a_h, h_g a_h$) and mass transfer coefficient ($K_m a_h$) which are obtained by Ben Amara et al. [5] and an algebraic equation of the curve of saturation of water steam [10]

$$h_l a_h = 25223.5 m_l^{0.0591} m_g^{0.1644} L^{-0.0542} \qquad (8)$$

$$K_m a_h = 0.6119 m_l^{0.1002} m_g^{0.3753} L^{-0.0986} \qquad (9)$$

The air–film voluminal heat transfer coefficient and the voluminal mass transfer on the air–water interface are related by Lewis relation [11], which is applicable to low concentration of water vapor in air provided

the area of heat and mass transfer are the same, as follows:

$$h_g = C_g K_m \tag{10}$$

The curve of saturation of water steam is given by the following equation:

$$W_I = 0.62198 \frac{P_I}{1 - P_I} \tag{11}$$

where P_I is the saturation pressure of the water vapor corresponding to a certain temperature is computed from [10] as follows:

$$\ln(P_I) = -6096.938 \frac{1}{T} + 21.240964 - 2.7111910^{-2}T$$
$$+ 1.6739510^{-5}T^2 + 2.43350 \ln(T) \tag{12}$$

4. Model approximation of humidifier

An analytical solution to Eqs. (1)–(4) is impossible, hence the equations must be discretized to obtain approximate, but still accurate, solutions. The method of finite differences has been used quite extensively in the past, but it usually requires a large number of discretization points and results in a correspondingly large set of ordinary differential equations (ODE). On the other hand, the orthogonal collocations method (OCM) approximates the solution by a polynomial trial function, and the resulting set of ODE is often considerably smaller. Currently, the collocation method is very widely used in chemical and biotechnological engineering problems [12,13].

4.1. Formulation of the approximation method

Consider the following partial differential equation (PDE):

$$\frac{\partial T}{\partial t} = f\left(x, t, T, \frac{\partial T}{\partial x}, \ldots\right) \tag{13}$$

with

- $t \in [0, t_f]$: time domain, $t_f < \infty$
- $x \in [x_0, x_l]$: spatial domain

To study a collocation method in this model, the following approximation series is used for the variable T:

$$\overline{T}(x, t) = \sum_{i=1}^{N} \chi_i(t) \varphi_i(x) \tag{14}$$

The specific method applied is called orthogonal collocation due to certain orthogonality properties of the base functions φ_i. Due to technical reasons, the number of the base functions is given in the form of $N + 2$. The points x_0 and x_{N+1} correspond to the initial and end points of the system. Consequently, the number of internal collocation points is N.

By using the Lagrange interpolation polynomial, L_j, as a base function, the Eq. (11) can be written as follows:

$$\overline{T}(x, t) = \sum_{j=0}^{N+1} L_j(x) T_j(t) \tag{15}$$

with

$$L_j(x) = \prod_{\substack{i=0 \\ i \neq j}}^{N+1} \left(\frac{x - x_i}{x_j - x_i}\right)$$

$$T_j(t) = \overline{T}(x = x_j, t)$$

x_j, $(j = 0, 1, \ldots, N+1)$: the collocation points.

With this method, the derivatives with respect to time and space are approximated as follows:

$$\frac{\partial \overline{T}(x, t)}{\partial t} = \sum_{j=0}^{N+1} L_j(x) \frac{dT_j(t)}{dt} \tag{16}$$

$$\frac{\partial \overline{T}(x, t)}{\partial x} = \sum_{j=0}^{N+1} \frac{dL_j(x)}{dx} T_j(t) \tag{17}$$

At the different collocation points, we can write:

$$\left.\frac{\partial \overline{T}(x, t)}{\partial t}\right|_{x=x_i} = \frac{dT_i(t)}{dt} \tag{18}$$

$$\left.\frac{\partial \overline{T}(x, t)}{\partial x}\right|_{x=x_i} = \sum_{j=0}^{N+1} l_{ij} T_j(t) \tag{19}$$

with

$$l_{ij} = \left.\frac{dL_j(x)}{dx}\right|_{x=x_i}$$

4.2. Application of the OCM

By substituting the approximations presented earlier in the initial system formed by partial derivatives equations, we can get a system of ordinary differential equations according to the time localized in every col-location point.

The set of PDEs is transformed to the following set of ODE using the OCM with the boundary conditions:
$$0 \leqslant x \leqslant L$$

$$T_l(L, t) = T_{l2}(t)$$
$$T_g(0, t) = T_{g1}(t)$$
$$W_g(0, t) = W_{g1}(t)$$

The expression of the humidifier-reduced dynamic model is given by the following equations:

$$\frac{dT_{li}}{dt} = \frac{m_l}{M_l} \left[\sum_{j=0}^{N} l_{ij} T_{lj} + l_{iN+1} T_{l2} \right] - \frac{h_l a_h}{M_l C_l} (T_I - T_{li}) \tag{20}$$

$$\frac{dT_{gi}}{dt} = -\frac{m_g}{M_g} \left[\sum_{j=1}^{N+1} l_{ij} T_{gj} + l_{i0} T_{g0} \right] - \frac{h_g a_h}{M_g C_g} (T_{gi} - T_I) \tag{21}$$

$$\frac{dW_{gi}}{dt} = -\frac{m_g}{M_g} \left[\sum_{j=1}^{N+1} l_{ij} W_{gj} + l_{i0} W_{g0} \right] + \frac{K_m a_h}{M_g} (W_I - W_{gi}) \tag{22}$$

$$h_l a_h (T_I - T_{li}) = h_g a_h (T_I - T_{gi}) + \lambda_o K_m a_h (W_I - W_{gi}) \tag{23}$$

$$W_I = 0.62198 \frac{P_I}{1 - P_I} \tag{24}$$

5. Simulation results and discussion

Simulation is the process of subjecting the model for a given thermal system to various inputs, such as operating conditions, to determine how it behaves and thus predict the characteristics of the actual physical system. Though simulation may be carried out with scale models and prototypes, the expense and effort involved generally makes it impossible to use these for design because many different designs and operating conditions need to be considered and evaluated. In this section, we describe the simulation results obtained when two types of disturbances occur. In the first disturbance, a change in the water temperature inlet is made, while in the second disturbance, a change in air temperature inlet is made.

5.1. Disturbance in water temperature inlet

Figs. 4 and 5 present the dynamic behavior of the outlet parameters of the humidifier ($T_{g2}(t)$, $T_{l2}(t)$ and $W_{g2}(t)$) further to a disturbance in water temperature inlet. Fig. 4 shows the dynamic behavior of air temperature and the corresponding absolute humidity at the outlet of the humidifier. It is clear from Fig. 4 that the fact of increasing inlet water temperature of 50% generates an increase of 22% of the air temperature and 34% rise in the air humidity. Following this perturbation of the water flow rate, the outlet water temperature undergoes an elevation nearly equal to 8.92% as shown in Fig. 5. This is due to the fact that increases in the inlet water temperature increases the gradient temperature between air and water inside the humidifier which in its turn leads to increasing the mass and heat transfer coefficients and then its outlet parameters. It is also noticeable from these simulation results that the air humidity is the most appreciable parameter to variation in inlet water temperature. Therefore, it is recommended to work with high inlet water temperature to guarantee high values of outlet air absolute humidity.

5.2. Disturbance in air temperature inlet

Fig. 6 presents the dynamic behavior of the outlet parameters of the humidifier ($T_{g2}(t)$, $T_{l2}(t)$ and $W_{g2}(t)$)
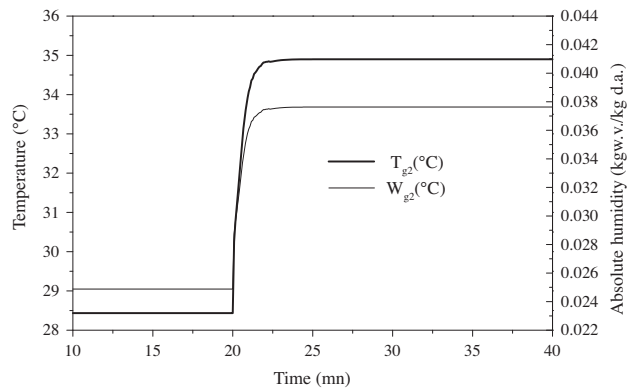

Fig. 4. Dynamic behavior of air temperature and air humidity at the humidifier exit further to a disturbance in water temperature inlet ($T_{g1} = 20$°C, $W_{g1} = 0.01488$ kg w.v./kg d.a. ($t \leqslant 20$ mn, $T_{l1} = 40$°C), ($t > 20$ mn, $T_{l1} = 60$°C)).
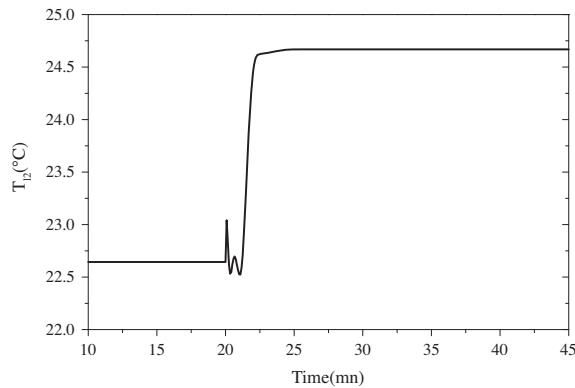
Fig. 5. Dynamic behavior of water temperature at the humidifier exit further to a disturbance in water temperature inlet ($T_{g1} = 20$ °C, $W_{g1} = 0.01488$ kg v./kg d.a. ($t \leqslant 20$ mn, $T_{l1} = 40$ °C), ($t > 20$ mn, $T_{l1} = 60$ °C)).
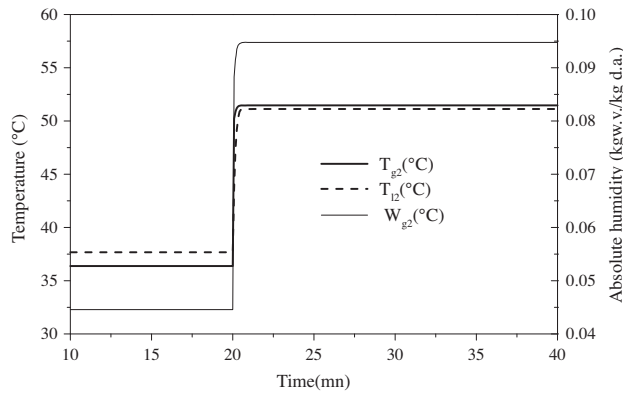

Fig. 6. Dynamic behavior of the humidifier outlet parameters further to a disturbance in air temperature inlet ($T_{l1} = 60$ °C, $m_1 = 0.1$ kg/s and $m_g = 0.2$ kg/s) ($t \leqslant 20$ mn, $T_{g1} = 30$ °C, $W_{g1} = 0.0275$ kg e./kg a.s.) ($t > 20$ mn, $T_{g1} = 50$ °C, $W_{g1} = 0.0875$ kg e./kg a.s.).

further to a disturbance in air temperature inlet. Simulation results show that a 66.66% rise in the humidifier inlet air temperature, $T_{g1}(t)$, yields a 41.47% elevation in $T_{g2}(t)$ and a 112.8% increase in $W_{g2}(t)$. Also, $T_{l2}(t)$ increases by 35.71%. Then, the absolute humidity at the humidifier exit is more sensible than the air and water outlet temperatures to the inlet air temperature. Therefore, according to these results, one can infer the interest of working with high values of air temperatures at the inlet of the humidifier to allow the latter to provide high values of absolute air humidity.

6. Experimental validation of the humidifier

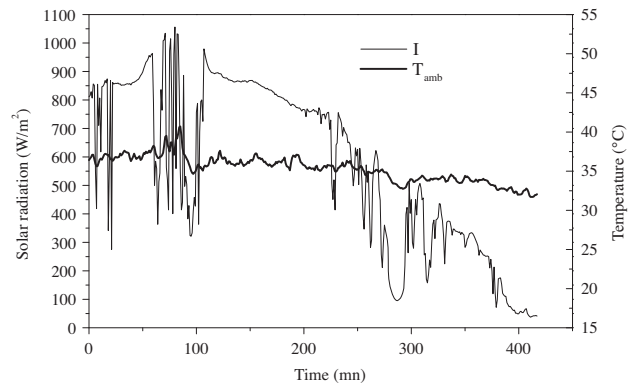The measured climatic conditions—solar radiation and ambient temperature for a typical day in August

Fig. 7. Climatic conditions measured during typical day in August.
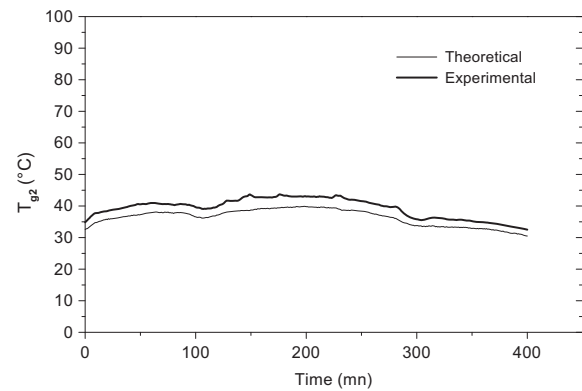

Fig. 8. Comparison between numerical and experimental values of air temperature at the humidifier exit.
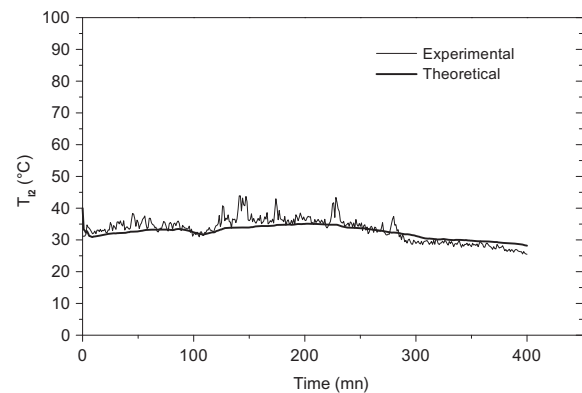

Fig. 9. Comparison between numerical and experimental values of water temperature at the humidifier exit.

(summer time) at the city of Sfax, Tunisia—are presented in Fig. 7. As shown in Fig. 7, the chosen day is characterized by high fluctuation of solar radiation. All the following figures of this paragraph refer to
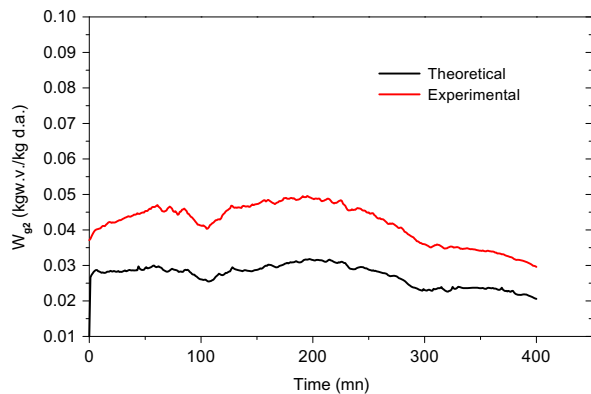
Fig. 10. Comparison between numerical and experimental values of moist air humidity at the humidifier exit.

these climatic conditions. To experimentally validate the developed mathematical model of the humidifier, the values of global solar radiation and ambient temperature were introduced to the simulation program as input data. For the experimental validation, all the measurements started at 10:00 a.m.

Figs. 8–10 present a comparison between the experimental and the theoretical values respectively of air and water outlet temperatures and the absolute humidity at the level of the humidifier. According to these figures, the experimental and simulation variations are identical for almost the entire time period. In addition, water and air outlet temperatures of the humidifier present only a small change during variation of the solar radiation for both experimental and numerical tests.

7. Conclusion

This paper presents theoretical and experimental studies of a pad humidifier used in solar desalination unit. To numerically simulate the humidifier in dynamic regime, we have developed a mathematical model based on heat and mass transfers between air and water inside the humidifier. The developed model is simulated, using the Borland C++ software to study the behavior of key output parameters. According to the simulation results, it is interesting to work with high values of both air and water temperatures at the inlet of the humidifier to allow the latter to provide high values of absolute air humidity.

The experimental validation revealed that the numerical prediction of the humidifier output parameters was in good agreement with the experimental values measured by sensors. This proves the validity of the mathematical model established for the humidifier

and the effectiveness of the orthogonal collocation method used to solve them. In addition, the validated mathematical model would help in the development of a computer-based design and simulation software for such type of humidifier.

Acknowledgements

Symbols

a	—	air–water exchanger area, m^2
C_g	—	air specific heat, J/(kg K)
C_l	—	water specific heat, J/(kg K)
h	—	heat transfer coefficient, J/(kg K)
h_g	—	air heat transfer coefficient at the air–water interface, (W/(m^2 K))
h_l	—	water heat transfer coefficient at the air–water interface, W/(m^2 K)
I	—	solar flux, W/m^2
K_m	—	water vapor mass transfer coefficient at the air–water interface (kg/(m^{2}s))
m	—	mass flow rate (kg/s)
M	—	mass (kg)
P_I	—	saturation pressure (Pa)
T	—	temperature (K)
W	—	air humidity (kg water/kg dry air)
W_I	—	saturation humidity (kg water/kg dry air)
L	—	length of the humidifier packed bed, m
x	—	coordinate in the flow direction (m)

Greek

λ_o	—	latent heat of water evaporation (J/kg)

Subscripts

1	—	humidifier inlet
2	—	humidifier exit
amb	—	ambient
l	—	liquid
g	—	moist air

References

[1] H.E.S. Fath, Desalination Technology. The Role of Egypt in Region, IWT C 2000, Alexandria, Egypt.

[2] Mohamed Aboudou Kassim, Brahim Benhamou, Souad Harmand, Effect of air humidity at the entrance on heat and mass transfers in a humidifier intended for a desalination system, Appl. Therm. Eng. 31 (2011) 1906–1914.

[3] Hichem Marmouch, Jamel Orfi, Sassi Ben Nasrallah, Experimental study of the performance of a cooling tower used in a solar distiller, Desalination 250 (2010) 456–458.

[4] K. Bourouni, M.T. Chaibi, Modelling of heat and mass transfer in a horizontal-tube falling film condenser for brackish water desalination in remote areas, Desalination 166 (2004) 17–24.

[5] Ben Amara, M. Houcine, I. Guizani, A.A. Guizani, M. Mâalej, Theoretical and experimental study of a pad humidifier used on an operating seawater desalination process, Desalination 168 (2004) 1–12.

[6] S. Yanniotis, K. Xerodemas, Air humidification for seawater desalination, Desalination 158 (2003) 313–319.

[7] K. Zhani, H. Ben Bacha, T. Damak, A study of a water desalination unit using solar energy, Desalin. Water Treat. 3 (2009) 261–270.

[8] K. Zhani, H. Ben Bacha, An approach to optimize the production of solar desalination unit using the SMCEC principle, Desalin. Water Treat. 13 (2010) 96–108.

[9] K. Zhani, H. Ben Bacha, Modeling and simulation of a new design of the SMCEC desalination unit using solar energy, Desalin. Water Treat. 21 (2010) 1–11.

[10] ASHRAE, Fundamental Handbook TomeV, 1977.

[11] M.A. Younis, M.A. Fahim, N. Wakao, Heat input-response in cooling tower-zeroth moments of temperature variations, J. Chem. Eng. Jpn. 20 (1987) 614–8.

[12] T. Damak, Modelling, evaluation and command of biotechnical processes of hyperbolic type, PhD Thesis, Universite Paul Sabatier, Toulouse, France, 1994.

[13] R.K. Srivastava, B. Joseph, Reduced-order model for separation columns. V. Selection of collocation points, Comput. Chem. Eng. 9 (1985) 601–613.